Available online at www.sciencedirect.com
ScienceDirect
Bioelectrochemistry 70 (2007) 155–164
Bioelectrochemistry
www.elsevier.com/locate/bioelechem

Interactions of adsorbed albumin with underpotentially deposited copper on gold piezoelectrodes

Maria Hepel *, Magdalena Stobiecka [1]

Department of Chemistry, State University of New York at Potsdam, Potsdam, NY 13676, USA

Received 26 August 2005
Available online 7 April 2006

Abstract

The adsorption of a model protein, bovine serum albumin (BSA), on Au electrodes was investigated using the Cu adatom probe method and Electrochemical Quartz Crystal Nanobalance (EQCN) technique. The adsorption of BSA was confirmed by AFM imaging and has been found to be controlled by kinetics. Using the Cu adatom probe method, we were able to reconstruct the entire BSA adsorption transient Θ_{BSA} vs. t. The adsorption rate constant k_1, determined from this transient is $k_1 = 2.45 \times 10^5$ L mol^{-1} s^{-1}. We have found that the bulk Cu^0 deposition process is blocked by BSA adsorption and it decays exponentially with time during BSA adsorption. It ceases completely when a full monolayer of BSA is formed. In contrast to that, the mass associated with Cu-u.p.d. decreases only to ca. 50% of that in the absence of BSA, indicating that Cu adatoms can penetrate (wedge) into the space between the surface Au atoms and the adsorbed BSA molecules. In addition to that, we have found that the degree of penetration of Cu adatoms can be controlled by the applied deposition potential. By selecting a sufficiently cathodic potential, we were able to deposit a full Cu-u.p.d. monolayer, independent of the BSA surface coverage extending from $\Theta_{BSA} = 0$ to $\Theta_{BSA} \approx 1$. The positive shift of Cu_{ad} desorption peak potential E_p, observed in the presence of adsorbed BSA, has been interpreted in terms of Frumkin exchange interaction forces between Cu_{ad} and BSA_{ad}, on the basis of our earlier theoretical model, expanded here to include adsorbed species in two monolayers. This expansion is possible owing to the fast rate of Cu adatom penetration in the interfacial region. From the plots of E_p vs. Θ_{BSA}, the presence of strong attractive interactions between Cu_{ad} and BSA_{ad} was deduced. These interactions result in a super-shift of the Cu-u.p.d. desorption peak potential, corresponding to the exchange interaction coefficient $g_{M,X} < -4$, indicating on a possibility of the formation of a stable interface complex.

Keywords: Albumin adsorption; BSA; EQCN; Metal adatom probe method; Cu-u.p.d.

1. Introduction

The adsorption of proteins on solid surfaces has been the subject of a particular scientific interest in many fields, including biomimetic electron-transfer processes [1–3], protein-membrane phenomena [4], studies of antibody–antigen and other affinity interactions [5–7], and the interactions of proteins with solid surfaces with various kinds of adsorbed species [8,9]. The interactions of proteins with metals have also been studied to investigate the effects of substrate materials on the protein molecule integrity and its biological activity [10–22]. The adsorption of proteins is an important issue for many practical applications such as the biosensors [7,23–29], medical implants [30], drug development and drug delivery systems [7,31], food processing [32–34], and others.

Among different methods used in studies of adsorbed proteins and other compounds of biological importance, are non-electrochemical techniques such as the radioactive labeling [35], ellipsometry [35–38], infrared reflection-absorption spectroscopy [39], electron microscopy [40], surface stress measurements [41], lateral friction force [42], electroreflectance [43] and surface-enhanced Raman spectroscopy [44]. A group of electrochemical methods includes voltammetry, used for studies of redox proteins [1–3], electrochemical quartz crystal nanobalance (EQCN) technique [26,45], adatom probe [8] and redox ion probe [9] methods, atomic force microscopy (AFM) [8,9,46], quartz crystal immittance (QCI) technique [9], rotating disk electrode (RDE) voltammetry [8], capacitance and surface charge measurements [1,47], and electrochemical impedance spectroscopy (EIS) [33]. The EQCN technique has been

* Corresponding author. Tel.: +1 315 267 2264; fax: +1 315 267 3170.
E-mail address: hepelmr@potsdam.edu (M. Hepel).
[1] On leave from Olsztyn University, Poland.

1567-5394/$ - see front matter © 2006 Elsevier B.V. All rights reserved.
doi:10.1016/j.bioelechem.2006.03.032

previously used to monitor a variety of surface processes [26], including adsorption and reactivity of small organic compounds of biological importance and biocompatible polymers [48–58]. Recent studies included also small polypeptides [48,49] and globular proteins [9,59,60].

In this work a model protein, bovine serum albumin (BSA), was used to study its adsorption on Au electrodes and surface interactions between underpotentially deposited copper adatoms and adsorbed BSA molecules. This experimental work is related to our earlier theoretical analysis [61] of the effect of irreversible adsorption of organic compounds on anodic stripping voltammetry of metals. In previous studies [8], we have investigated the kinetics of BSA adsorption on a Ag-RDE using the Pb-adatom probe technique in the range of low BSA surface coverages, $0<\theta_{BSA}<0.4$. It has been found that the adsorption process is relatively fast, with the rate constant: $k_{ads}=2.42\times10^{-4}$ cm/s. The equilibrium constant for BSA adsorption on Ag electrode is: $K_{ads}=2.17\times10^{7}$ L/mol, which corresponds to the Gibbs free energy of adsorption: $\Delta G^{0}_{ads}=-9.99$ kcal/mol (−41.85 kJ/mol). The adsorption of BSA on Au is also relatively strong, as documented in EQCN and AFM studies [9]. Recently [9,62], we have investigated the conformational transitions of BSA molecules adsorbed on Au using the EQCN and QCI techniques. The conformational transitions were induced under potential control conditions by Cd adatoms and the electrocatalytic nitrate reduction process.

To gain further insight into the nature of metal adatom interactions with adsorbed proteins, in the present work we have investigated the surface phenomena associated with adsorbed BSA and Cu adatoms, which do not induce conformational transitions observed with underpotentially deposited cadmium [9]. The particular interest was whether the Cu_{ad} adatoms do interact with BSA_{ad} and whether they can wedge into the space between the surface Au atoms and the adsorbed BSA molecules. This type of wedging process was suggested before for copper metal adatoms and adsorbed tripeptide glutathione [48,49], as well as for Cu-u.p.d. and self-assembled monolayer films of short carbon chain thiols [63].

2. Experimental

2.1. Chemicals

All chemicals used for investigations were of reagent grade purity. Bovine serum albumin (BSA) was purchased from Aldrich Chemical Company and was used without further purification. The molar mass of BSA is $M_{BSA}=69{,}000$. Other compounds, including copper sulfate and sulfuric acids, were obtained from Alfa Aesar. Solutions were prepared using Milli-Pore Milli-Q deionized water (conductivity $\sigma=55$ nS/cm). They were deoxygenated by bubbling with purified nitrogen. The experiments were performed at room temperature, 22 °C.

2.2. Instrumentation

An Electrochemical Quartz Crystal Nanobalance Model EQCN-930 (Elchema, Potsdam, NY) with 10 MHz AT-cut quartz crystal resonators was used in this study. The EQCN technique allowed us for simultaneous monitoring of voltamperometric and nanogravimetric characteristics. The resonant frequency of the quartz crystal lattice vibrations in a thin quartz crystal wafer was measured as a function of the mass attached to the crystal interfaces. For thin rigid films, the interfacial mass changes Δm were related to the shift in series resonance oscillation frequency Δf of the EQCN through the Sauerbrey equation [64]:

$$\Delta f = -\frac{2\Delta m n f_0^2}{A\sqrt{\mu_q \rho_q}} \quad (1)$$

where f_0 is the oscillation frequency in the fundamental mode, n is the overtone number, A is the piezoelectrically active surface area, ρ_q is the density of quartz ($\rho_q=2.648$ g cm^{-3}), and μ_q is the shear modulus of quartz ($\mu_q=2.947\times10^{11}$ g cm^{-1} s^{-2}). The oscillator was tuned to the resonance frequency of working piezoelectrodes to minimize effects due to energy dissipation in protein films. All experimental variables influencing the resonant frequency [26] of the EQCN electrodes, such as the temperature, pressure, viscosity and density of the solution, were kept constant during the course of measurements. The experimental uncertainty in the apparent mass change measurements was ±0.1 to ±0.5 ng (depending on the time scale of experiments) and the instrument resolution was 0.01 ng.

The piezoelectrically active (geometrical) surface area of the working Au electrode was 0.196 cm^2 and the real surface area $A=0.255$ cm^2 (roughness factor $R=1.3$). A 200 nm thick Au film was deposited on a 14-mm diameter, 0.166-mm thick, AT-cut quartz resonator wafer with vacuum evaporated Cr adhesion interlayer (20 nm thick). The real surface area was determined for Au-EQCN electrodes by a standard monolayer oxide formation procedure [65].

The resonator crystals were sealed to the side opening in a glass vessel of 50 mL capacity using high purity siloxane glue with intermediate viscosity (Elchema SS-431). The seal was cured for 24 h at room temperature. The working electrode was polarized using a Pt wire counter electrode and its potential measured vs. a double-junction (1 M KNO_3 external solution) KCl saturated Ag/AgCl electrode.

A Model PS-605 potentiostat/galvanostat (Elchema) was used in the measurements. A 16-bit real-time Data Logger and Control System DAQ-716v with VOLTSCAN 5.0 (Intellect Sft., Potsdam, NY) working under MS Windows-XP operating system was used for simultaneous recording of i–E and Δf–E, or i–t and Δf–t curves. The experimental curves were fitted using Voltscan 5.0 or Microcal Origin 6.0 least-square fitting routines. For fitting of adsorption kinetics transients, appropriate equations were programmed as the user-defined functions.

Atomic Force Microscopy (AFM) imaging of BSA films on Au piezoelectrodes was done using a Veeco Model Nanoscope IIIa SPM and an Elchema nanopositioner Nanoscan NP-5.03. The cantilevers with high resonance frequency (higher than 250 kHz) with sharpened Si tips for tapping mode AFM imaging were employed.

2.3. Procedures

The Au electrode surface was cleaned by degreasing in propyl alcohol, followed by immersing in piranha etching solution

(30% H_2O_2/H_2SO_4=1:3) for 2 min, and rinsing with triply distilled water. The Au|BSA films were formed by injection of an aliquot of 0.1% w/w BSA stock solution (14.49 μM) into the analyte under study while monitoring the EQCN frequency shift and/or the decay of a redox ion probe current using cyclic voltammetry. The BSA concentrations, after dilution, were in the range from 4.8×10^{-8} to 6×10^{-7} M. The permeability of BSA films was tested using a Cu adatom probe method or occasionally a redox probe method with 0.4–3 mM $Fe(CN)_6^{3-}$ ion probe solution, except as otherwise noted. The electrolyte concentrations employed during BSA film formation and experiments with Cu deposition were maintained low to avoid suppression of electrostatic components of BSA–BSA and BSA–substrate interactions. The main solution used for investigations of BSA dynamics was 5 mM $CuSO_4$+5 mM H_2SO_4 with pH=2.19, which was used in all experiments, except as otherwise noted. In this solution, BSA is in a partially unfolded (denatured) state [62] (the native state can be reversibly restored at higher pH and higher salt concentration). The medium exchange, whenever necessary, was done without drying the protein film. All experiments were carried out with freshly prepared Au|BSA electrodes (within 2–3 h from the film deposition) to avoid long term conformation changes of adsorbed BSA, which may be encountered at longer times (e.g. overnight).

The acoustic impedance characteristics vs. frequency in vicinity of resonance and antiresonance frequency were recorded using QCI unit of the Model EQCN-930 employing the procedure described earlier [9,66]. The high frequency complex admittance (10 MHz band) of quartz crystal resonators was analyzed using evaluation and simulation functions of Voltscan QCI 2.0 software. The adsorption of BSA on Au piezoelectrodes caused only a minor increase in the resonance resistance (less than 2 Ω). Hence, the BSA film can be treated as a thin rigid film. The admittance characteristics of BSA films on Au are published elsewhere [9]. No changes in the admittance modulus vs. frequency characteristics were observed on deposition of small amount of copper, investigated in this work.

The BSA films for AFM imaging were prepared in the same way as for the EQCN measurements, viz. by injection of a 9.6×10^{-8}M BSA to a solution with submerged substrate for 60 min, followed by washing with distilled water and drying with a stream of nitrogen at room temperature.

3. Results and discussion

3.1. Effect of albumin on bulk-Cu deposition on Au electrode

The adsorption of BSA on a gold electrode results in the partial blocking of electrode surface. The diminished accessibility of electroactive species to charge transfer centers can be used to evaluate the degree of surface coverage by BSA. In Fig. 1, the effect of BSA on linear scan voltammetric characteristics of a Au electrode in 5 mM $CuSO_4$+5 mM H_2SO_4 solution after injection of a 9.6×10^{-8}M BSA, is presented for scan rate ν=50 mV/s. During the course of BSA adsorption, the active surface area of Au electrode is gradually diminished and, hence, the Cu^{2+} discharge currents decrease in consecutive curves ob-

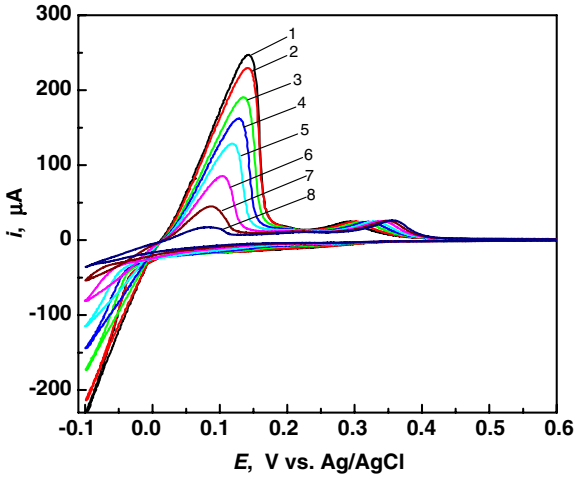

Fig. 1. Linear potential scan voltammograms for a Cu^0 deposition and electrodissolution obtained in a 5 mM $CuSO_4$+5 mM H_2SO_4 solution, recorded at ν=50 mV/s, before and after injection of a 9.6×10^{-8}M BSA; BSA adsorption time [min]: (1) 0, (2) 0.15, (3) 1, (4) 2, (5) 3, (6) 4, (7) 5, (8) 6.

tained at longer times of BSA adsorption. At the same time, the Cu^0 electrooxidation peak height also decreases, confirming the lower amounts of copper deposited. The mass of Cu^0 formed in these experiments was monitored by recording the EQCN resonant frequency changes. The graph of Cu^0 mass $m_{Cu,bulk}$ vs. time of BSA adsorption $t_{ads,BSA}$ is presented in Fig. 2. The $m_{Cu,bulk}$–$t_{ads,BSA}$ curve can be fitted with empirical single exponential decay function:

$$m_{Cu,bulk} = m_{fin} + A\exp\left\{-\frac{t_{ads,BSA}}{\tau_0}\right\} \quad (2)$$

where m_{fin} is the final mass (m_{fin}=1.58 ng), A is the amplitude (A=169.4 ng), and τ_0 is the characteristic time constant for the mass decay (τ_0=3.12 min). It is seen that at times longer than 18 min (ca. $6\times\tau_0$), the Au surface is virtually completely blocked to the bulk Cu^0 deposition process. Therefore, the probing test with bulk Cu^0 deposition can basically be used to estimate the surface coverage Θ_{BSA} by adsorbed BSA. However, in order to do that, the linearity of the dependence $\Theta_{BSA}=f(m_{Cu,upd})$, or exact form of this dependence if it is non-linear, should be tested. Although the experimental $m_{Cu,bulk}$ and $i_{p,Cu,bulk}$ correctly decrease to zero on adsorption of BSA, we have to take into account the fact that in the growth of 3-D nuclei of Cu^0, both the current and mass are related to the projected surface area as follows:

$$m_{Cu,bulk}\,\alpha V_{Cu} = \frac{1}{2}\left(\frac{4}{3}\pi r^3\right) = \frac{2}{3}Ar = \frac{2}{3\sqrt{\pi}}A^{3/2}, \quad (3)$$

if we assume a simple model of monodispersed Cu^0 nuclei with a hemispherical shape. In the above expressions, V_{Cu} is a volume and A is a cross section of the nucleus. Therefore, $m_{Cu,bulk}$ should show an inherent superlinear dependence on A. The same type of a relationship is expected between $i_{p,Cu,bulk}$ and A. In reality, the situation becomes more complicated because the nuclei are usually polydispersed and the shape of nuclei may vary. The theory and experimental evidence for the non-linearity of the charge–time transients for progressive nucleation processes were published

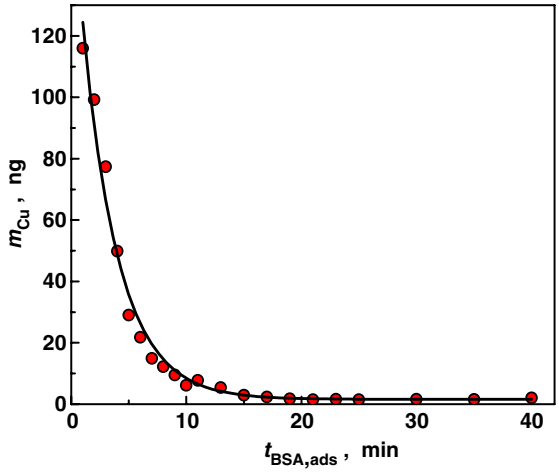

Fig. 2. The $m_{Cu,bulk}$ vs. $t_{ads,BSA}$ plot for the EQCN mass of Cu^0 deposited on a Au piezoelectrode from 5 mM $CuSO_4$+5 mM H_2SO_4 solution, by scanning to E_{dep}=−0.1 V vs. Ag/AgCl at v=50 mV/s, as a function of BSA adsorption time after injection of a 9.6×10^{-8} M BSA; solid line represents the exponential decay fitting function.

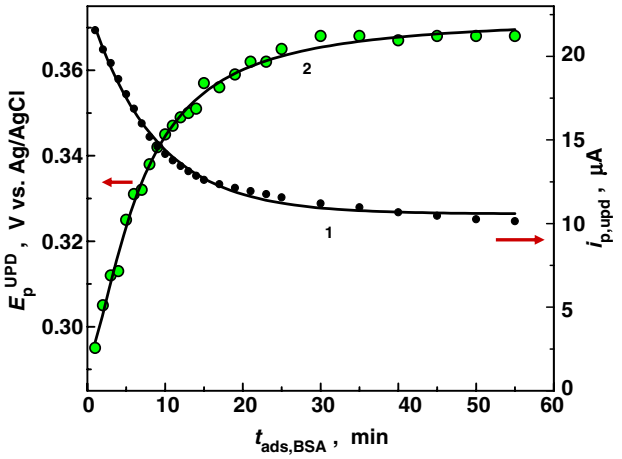

Fig. 4. The time dependence of: (1) peak current $i_{p,upd}$ and (2) peak potential E_p^{upd}, for the desorption of a Cu-u.p.d. formed during the adsorption process of BSA on a Au electrode; conditions the same as for Fig. 3; solid lines: non-linear LSQ fitting.

elsewhere [67]. This means that the calculation of Θ_{BSA} from the bulk Cu deposition characteristics is not as straightforward as it might seem at the first glance. Since, in contrast to the bulk metal probes, the adatom probes form only a monolayer coverage, they are free from 3-D nucleation problems of the bulk metal probes, we will rely more on the adatom probes, evaluated in the following sections. The bulk Cu^0 probe will be employed to confirm the full coverage of BSA.

3.2. Formation of Cu-u.p.d. on Au in the presence of adsorbed albumin

The u.p.d.-Cu on gold, which is observed in the absence of BSA, is also formed in the presence of BSA. We have found that in contrast to the bulk Cu^0 deposition, the u.p.d.-Cu process

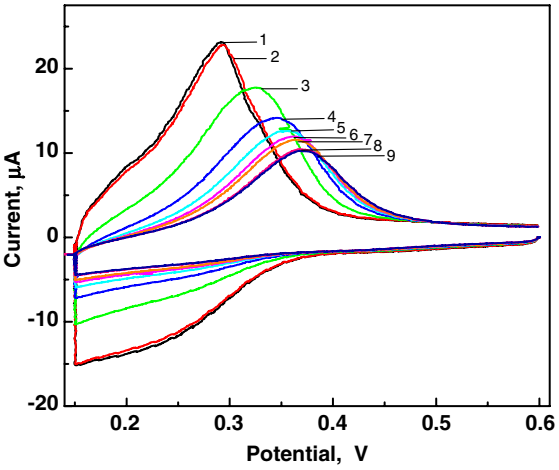

Fig. 3. Voltammograms for Cu-u.p.d. formation and stripping in a 5 mM $CuSO_4$+5 mM H_2SO_4 solution; Cu-u.p.d. deposited potentiostatically at E_{dep}=+0.15 V vs. Ag/AgCl for τ_{dep}=5 s, recorded at v=50 mV/s, before and after injection of a 9.6×10^{-8} M BSA; BSA adsorption time [min]: (1) 0, (2) 0.15, (3) 5, (4) 10, (5) 15, (6) 21, (7) 25, (8) 45, (9) 50.

does not vanish completely at high BSA surface coverage. Therefore, we have investigated this interesting phenomenon in more details. In Fig. 3, a series of voltammograms for u.p.d.-Cu formation and stripping are presented. The program waveform included a potential scan from E_1=0.6 V to E_2=0.15 V at v=50 mV/s, holding at E_2=0.15 V for τ_{dep}=5 s, and a scan to E_3=0.6 V at v=50 mV/s. The test voltammograms were recorded before BSA injection and periodically after the injection of 9.6×10^{-8} M BSA. It is seen that the anodic Cu desorption peak current $i_{p,Cu\text{-}upd}$ decreases during the adsorption of BSA and simultaneously, the peak potential $E_{p,Cu\text{-}upd}$ shifts toward more positive values. However, the $i_{p,Cu\text{-}upd}$ does not decrease down to zero, even after 60 min of BSA adsorption. The peak current decay plot of $i_{p,Cu\text{-}upd}$ vs. $t_{ads,BSA}$ is presented in Fig. 4, curve 1. The solid line represents a nonlinear least-square (LSQ) fitting to the exponential decay function: $i=i_{fin}+A\exp\{-t/\tau_0\}$, with i_{fin}=10.58 μA, A=12.55 μA, and τ_0=8.43 in. At $\Theta_{BSA}\approx1$, the peak current actually decreases only to ca. 50% of the initial value. In comparison to that, the bulk Cu^0 deposition decreased to ca. 2% of its initial value, for the same Θ_{BSA}. Therefore, it is possible that part of the u.p.d.-Cu may be wedged into the space between the Au surface atoms and the adsorbed BSA molecules.

It has to be pointed out that it is not only the bulk Cu^0 mass, which decreases to zero at $t_{ads,BSA}$>18 min, that makes us believe that a full monolayer coverage of BSA has been achieved. We have also an independent confirmation from AFM imaging, which indicates that a full monolayer coverage of BSA is developed on samples showing high penetration of Cu adatoms. An example of an AFM image of such a Au|BSA electrode surface is presented in Fig. 5. The AFM image was obtained using a Si tip oscillating at 273 kHz, in the constant amplitude negative feedback mode (also called the tapping mode) to avoid any effect of the scanning tip on the soft BSA film. The tapping mode is well established for studies of soft targets. The AFM image presented in Fig. 5 shows the edge of a dense BSA film. The sectioning analysis of the film thickness

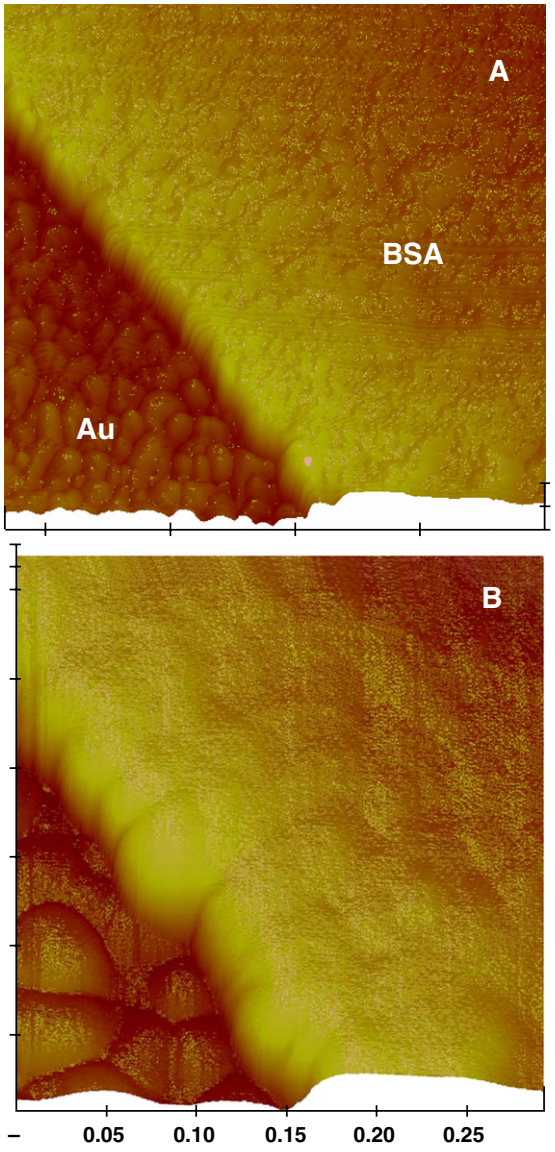

Fig. 5. Tapping mode AFM image of the edge of a BSA adsorption film on Au piezoelectrode obtained from a 5 mM $CuSO_4$+5 mM H_2SO_4+9.6×10^{-8} M BSA solution after 60 min of BSA adsorption; image size: (A) 875×875 nm^2, (B) 280×280 nm^2; vertical sensitivity 5 nm/div.

indicates that the height is h=4 nm, which corresponds to the height of BSA molecules in horizontal orientation. Single molecules of BSA observed in other media [9], could not be resolved here, most likely because of the partial melting of the protein at the low pH of the solution (conformer F with partially unfolded domain III). We have not observed any Cu^0 clustering on top of the BSA film, which appeared to be very smooth.

The peak potential shift for u.p.d. desorption is shown in Fig. 4, curve 2. It can be fitted with the empirical logistic function:

$$E_p = \frac{E_1 - E_2}{1 + \left(\frac{t_{ads,BSA}}{t_0}\right)^p} + E_2 \qquad (4)$$

with E_1=0.292 V, E_2=0.372 V, t_0=6.70, and p=1.56. It has to be noted that any binding of Cu^{2+} to BSA in solution [68] would cause a decrease of the Cu(II) discharge potential and a negative shift of E_p. In our experiments, to the contrary, not a negative shift but positive shift of the peak potential is observed. The positive shift indicates on some kind of hindrance of removal of Cu adatoms from Au surface at higher Θ_{BSA}. However, these difficulties are not due to any kinetic retardation of the desorption process or mass transport slowness since this would immediately be manifested by the strong asymmetry of desorption peak, which is not observed on any curve (Fig. 3). Evidently, the shift of E_p must be associated with surface interactions of Cu adatoms with adsorbed BSA. Further analysis of these interactions is presented in the next section.

3.3. Surface interactions of Cu_{ad} with adsorbed BSA

The interactions of Cu_{ad} with adsorbed BSA can be related to the model of lateral interactions of organic species with metal adatoms, which we have developed before [61] for stripping voltammetry. On the basis of Frumkin interaction forces, the desorption peak of a metal u.p.d. (M_{ad}) should be shifted negatively when repulsive forces between M_{ad} and the adsorbed organic X_{ad} are present. Alternatively, the M_{ad} desorption peak should be shifted positively when atractive forces between M_{ad} and the adsorbed organic X_{ad} are dominant. The relationships between the peak potential E_p and system parameters are complex. For a potentiostatic metal adatom deposition followed by linear scan anodic stripping, we have derived the following formula:

$$E_p = E^{0,f} + \frac{RT}{\alpha zF}\ln\left(\frac{\alpha v}{k_s}\right) + \frac{RT}{\alpha zF}\ln\left(-\frac{Q_{mono}}{RT}\right) - \frac{RT}{zF}g_{M,X}\Theta_X \qquad (5)$$

where $E^{0,f}$ is the formal standard potential for M/M^{z+} couple, z is the metal ion charge, α_{an} ia the charge transfer coefficient, k_s is the standard rate constant, v is the potential scan rate, Q_{mono} is the monolayer charge, $g_{M,X}$ is the exchange interaction coefficient

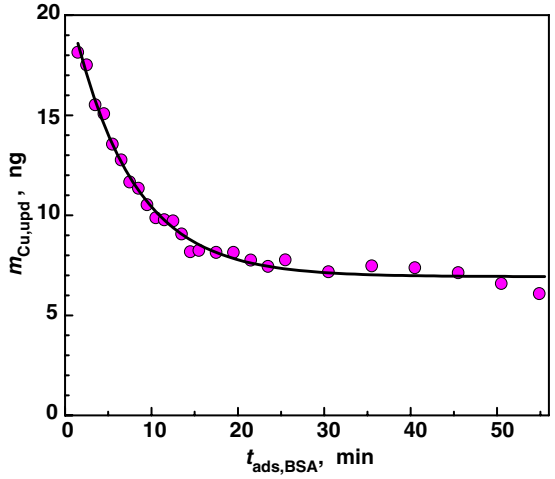

Fig. 6. The $m_{Cu,upd}$ vs. $t_{ads,BSA}$ plot for the mass of a Cu-u.p.d. formed during the adsorption process of BSA on a Au electrode; conditions the same as for Fig. 3; solid line represents a nonlinear LSQ fitting to the exponential decay function.

between M_{ad} and X_{ad}, and Θ_X is the surface coverage by X_{ad}. In our case, $E^{0,f}$ includes also the term due to the Gibbs free energy of M-u.p.d. formation on the given substrate, ΔE^0_{upd}. By rearrangement, Eq. (5) can be presented in the form:

$$E_p = E' + \frac{RT}{\alpha zF}\ln(v) - \frac{RT}{zF} g_{M,X}\Theta_X \quad (6)$$

where E' is a constant. From this equation, it becomes clear that at a constant scan rate, the peak potential for M_{ad} desorption is directly related to the exchange interaction coefficient $g_{M,X}$ and the surface coverage by organic compounds Θ_X. To determine the kind and strength of interaction forces between M_{ad} and X_{ad}, we can plot E_p versus Θ_X and obtain the interaction coefficient $g_{M,X}$ from the slope:

$$\left(\frac{\partial E_p}{\partial \Theta_X}\right)_v = -\frac{RT}{zF} g_{M,X} \quad (7)$$

Since the Θ_X values are usually not directly known, we can use the probe current or adatom mass to determine these values. Here, we have a choice of $i_{p,Cu,bulk}$, $i_{p,Cu,upd}$, $m_{Cu,bulk}$, and $m_{Cu,upd}$. As discussed earlier, we will rely more on the adatom probes due to the expected superlinear dependence of bulk Cu functions on free surface area (Eq. (3) and the problem of *incubation* time due to the nucleation and growth effects [67]). Therefore, we utilize here the u.p.d. mass data to evaluate Θ_{BSA}. The Cu adatom probe variables (especially, $m_{Cu,upd}$) should be linear with the accessible surface area ($1-\Theta_{BSA}$). In an ideal case, one would expect then that $m_{Cu,upd}$ should cease to zero when $\Theta_{BSA}\rightarrow 1$. As seen in Fig. 6, this is not happening in our experiments despite that the Cu bulk probe tests indicate a full blocking effect by BSA. In Fig. 6, the $m_{Cu,upd}$ vs. $t_{ads,BSA}$ experimental data are fitted with an exponential decay function (solid line): $m = m_{fin} + A\exp\{-t/\tau_0\}$, with $m_{fin} = 6.89$ ng, $A = 13.43$ ng, and $\tau_0 = 7.05$ min. The only plausible explanation of high final mass of Cu-u.p.d. m_{fin} is that Cu adatoms may still be able to penetrate the interface Au|BSA by wedging into the space between Au surface atoms and the adsorbed BSA molecules, while there is no other mechanistic pathway to form 3D Cu^0 nuclei, other than on an uncovered Au surface. Similar effects were considered in thiol SAM's by Espandiu et al. [63] and in systems of small adsorbed biological molecules [48,49,69].

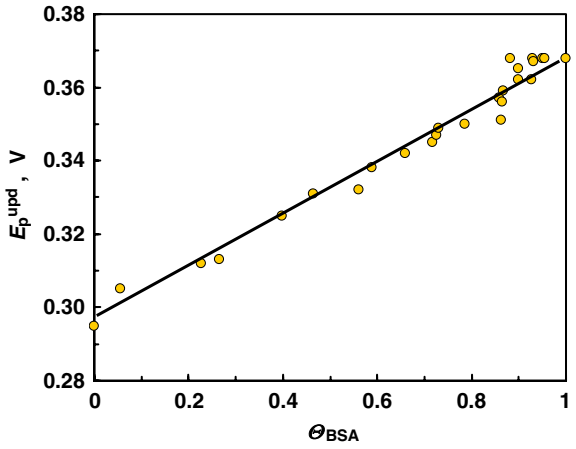

Fig. 8. Plot of E_p^{upd} vs. surface coverage of BSA Θ_{BSA} obtained from a single experiment during BSA adsorption on a Au piezoelectrode from a solution of 5 mM $CuSO_4$ + 5 mM H_2SO_4 + 9.6×10^{-8} M BSA.

To test the above conclusions, we can return back to Eq. (6) and note that E_p should be a linear function of Θ_{BSA}. Thus, if $m_{Cu,upd}$ is really a measure of Θ_{BSA}, then E_p should be a linear function of $m_{Cu,upd}$. The plot of E_p vs. $m_{Cu,upd}$ is presented in Fig. 7 and shows a well defined linear dependence. On the other hand, if we plot E_p vs. $m_{Cu,bulk}$ or E_p vs. $i_{p,Cu,bulk}$ (plots not shown) then we do not obtain linear dependencies, as expected. Therefore, we can conclude that $m_{Cu,upd}$ can be used to calculate Θ_{BSA}. In further investigations, we have employed the following definition for Θ_{BSA}:

$$\Theta_{BSA} = 1 - \frac{(m_{Cu} - m_{Cu,min})}{(m_{Cu,max} - m_{Cu,min})} \quad (8)$$

Using this extended definition, we can now plot the Cu_{ad} desorption peak potential E_p vs. Θ_{BSA}. This plot is shown in Fig. 8. The slope $(\partial E_p/\partial\Theta)_v = 0.0718$, hence the value of $g_{M,X} = -2.80$, indicating strong attractive interactions between the

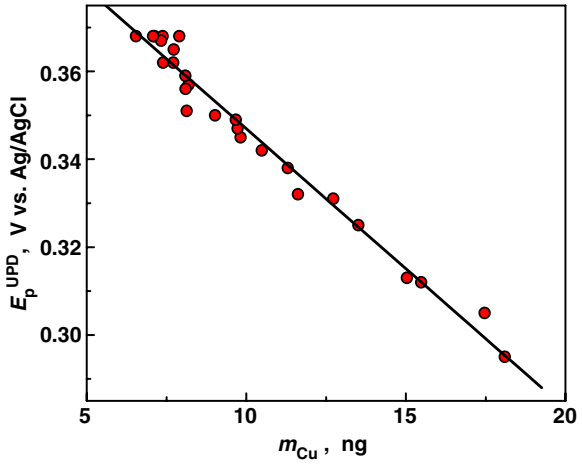

Fig. 7. Plot of the peak potential E_p^{upd} vs. mass of Cu-u.p.d. $m_{Cu,upd}$ observed during the adsorption of BSA on a Au piezoelectrode from a solution of 5 mM $CuSO_4$ + 5 mM H_2SO_4 + 9.6×10^{-8} M BSA.

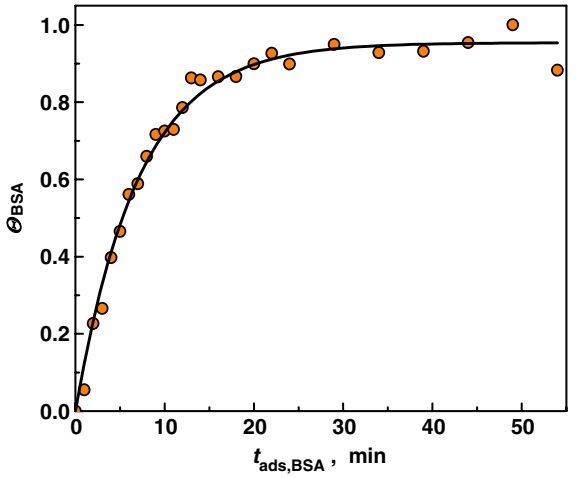

Fig. 9. The BSA adsorption transient Θ_{BSA} vs. $t_{ads,BSA}$ reconstructed from measurements of EQCN mass of a Cu-u.p.d. formed on a Au|BSA electrode during BSA adsorption.

adsorbed BSA and Cu_{ad}. For the sake of comparison, we can invoke similar investigations we have performed with BSA and Pb-u.p.d. on Ag-RDE [8], which have shown that the interactions of adsorbed BSA with Pb_{ad} are very weak and $g_{M,X} \approx 0$.

Using the BSA surface coverages determined from Cu-u.p.d. mass data, the adsorption transient Θ_{BSA} vs. t can now be reconstructed, as shown in Fig. 9. The experimental transient is fitted (solid line) with the adsorption kinetics function:

$$\Theta_{BSA} = \Theta_{eq}\left(1-\exp\left\{-\frac{t}{\tau_0}\right\}\right) \quad (9)$$

with $\Theta_{eq}=0.954$, and time constant $\tau_0=7.07$ min. Here, $\tau_0=1/(k_1C+k_{-1})$, where k_1 and k_{-1} are the adsorption and desorption rate constants, respectively, and C is the BSA concentration in solution. The initial slope of adsorption transient is: $(\partial\Theta/\partial t)_{t=0}=0.141$ min^{-1}. From this slope, the value of k_1 can be evaluated since: $(\partial\Theta/\partial t)_{t=0}=k_1(1-\Theta)C$. Hence, for $\Theta=0$ at $t=0$, one obtains: $k_1=1.47\times10^6$ L/(mol min)$=2.45\times10^5$ L/(mol s).

3.4. Further insights into the formation of Cu-u.p.d. and interactions with adsorbed albumin

The process of wedging of Cu_{ad} into the space between the surface gold atoms and the adsorbed BSA molecules, mentioned earlier, is difficult for detailed studies. In particular, the assessment of surface density of $Cu_{ad,w}$ of copper adatoms underneath BSA is not well understood. On the basis of the $m_{Cu,upd}$ measurements (Fig. 6), it is seen that the surface coverage of Cu_{ad} is close 0.5 at $\Theta_{BSA} \approx 1$. In other words, copper adatoms underneath adsorbed BSA molecules fill only about half of adsorption sites that would otherwise be filled on an uncovered Au surface.

To gain more information on Cu_{ad} wedging process, we have performed a series of experiments similar to those shown in Fig. 1,

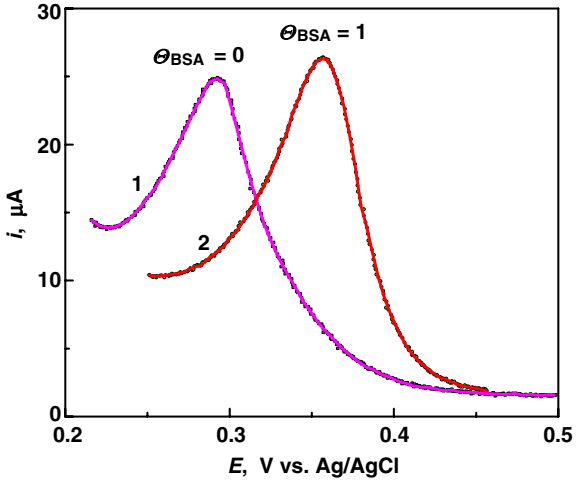

Fig. 10. Voltammetric desorption peaks of a full monolayer Cu-u.p.d. formed on: (1) bare Au and (2) Au|BSA electrode, in a solution of 5 mM $CuSO_4$+5 mM H_2SO_4; solution contained also 9.6×10^{-8} M BSA for curve (2); $v=50$ mV/s, $E_{dep}=-0.1$ V, $\tau_{dep}=1$ s.

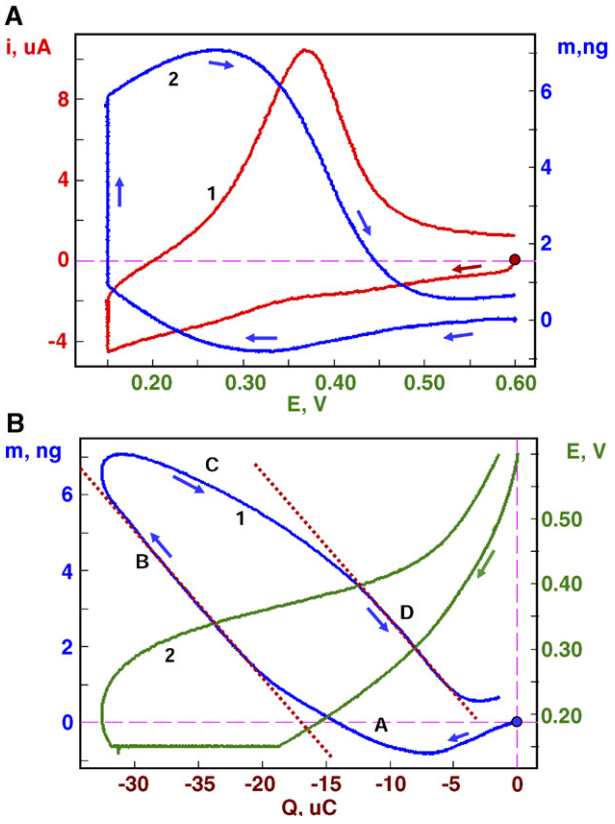

Fig. 11. (A) The EQCN characteristics: (1) i–E and (2) m–E, for the Cu-u.p.d. formation and stripping on a Au|BSA piezoelectrode in 5 mM $CuSO_4$+5 mM H_2SO_4+9.6×10^{-8} M solution. (B) The m–Q analysis (1) on the basis of the above data (see text for explanation of symbols); the E–Q plot (2) is provided to reference the charge to potential.

in which the Cu-u.p.d. desorption peak was recorded before and after the injection of 9.6×10^{-8} M BSA. The test waveform involved a potential scan to $E=-0.1$ V so that in every test a bulk Cu^0 was always formed. In the return potential scan, after dissolution of bulk Cu^0, we recorded the Cu-u.p.d. peak. We have found that the peak current and charge for the Cu_{ad} desorption remain approximately the same. At the same time, the peak potential shifts positively by $\Delta E_p=66$ mV after BSA adsorption, as shown in Fig. 10. The invariance of desorption charge means that by forcing the deposition of bulk Cu^0 by applying sufficiently cathodic potential, the Cu-u.p.d. could be formed with filling all active centers on Au surface, similar as in the absence of BSA. Therefore, we were able to attain a full Cu_{ad} coverage $\Theta_{Cu,upd} \approx 1$ under a full BSA film with $\Theta_{BSA} \approx 1$. As far as we know, this is the first observation of metal adatoms wedging underneath an adsorbed protein film.

The observations of a 0.5 monolayer coverage of Cu_{ad} in data presented in Fig. 6 and full monolayer coverage in experimental data presented in Fig. 10 are not contradictory. We can rationalize these two observations by realizing that the time scale and value of the deposition potential were different in these measurements. While in the former case (Fig. 6) only a short deposition time at relatively high potential was applied, the scan to a much more negative potential was used in the latter case (Fig. 10). Obviously, the wedging process of Cu_{ad} requires more

time and lower potentials for the completion. To evaluate the role of these two variables (i.e. time and potential), we have to invoke once again the experiments of Fig. 6. The variation of the $m_{Cu,upd}$ with BSA adsorption time ceases after ca. 18 min and $m_{Cu,upd}$ approaches a constant value. Evidently, at the deposition potential $E=+0.15$ V, the wedging can not progress any further. Therefore, it is the selection of a proper deposition potential that is needed for further progressing of the Cu_{ad} wedging process into the space between surface Au atoms and the adsorbed BSA molecules. The possibility of wedging metal adatoms beneath the thiol SAM's was considered by Czanderna et al. [70,71] and demonstrated by Espandiu et al. [63] for Cu-u.p.d. on Au(111), while Eliadis et al. [72] in galvanostatic experiments found a low density of Cu clusters on top of a short chain thiol monolayer. It is interesting that the buried Cu-u.p.d. investigated by Espandiu et al. [63] has shown a positive shift of the desorption peak potential E_p with respect to that on a bare Au(111) surface, with $E_p=+0.39$ V (vs. Ag/AgCl) for Cu-u.p.d. buried beneath the ethanethiol monolayer. Similar to the observations of Espandiu et al. [63], we have also found in our experiments a positive shift of E_p, which increased gradually from +0.295 V to +0.370 V with increasing surface coverage of BSA from $\Theta_{BSA}=0$ to $\Theta_{BSA}\approx 1$. The evaluation of the strength of interactions between Cu_{ad} and adsorbed BSA using Eq. (6) leads to $g_{M,X}=-2.8\,z$. By substituting $z=2$, one obtains $g_{M,X}=-5.6$, which is less than the critical value $g^*=-4$ setting the boundary for a new compound or phase formation. However, if a new compound or phase would be formed, e.g. in the process:

$$p\mathrm{Cu}^{2+}_{(aq)} + \mathrm{BSA}_{ad} + 2p\mathrm{e}^- = \mathrm{Cu}_p\mathrm{BSA}_{(s)} \qquad (10)$$

then both the Nernstian equilibrium potential E_{eq} and E_p for the oxidation of Cu_pBSA would be expected to show a shift: $(\partial E_p/\partial\Theta)=RT/(2F)=0.0128$ V in the quasi-reversible case, or: $(\partial E_p/\partial\Theta)=RT/(\alpha F)\approx 0.0514$ V in the irreversible case. The E_p shift observed experimentally is much larger, $(\partial E_p/\partial\Theta)=0.072$ V. This supershift of E_p may be due to the surface supersaturation and partial charge transfer. Experimental measurements of the latter are difficult due to the two-step electrode reaction of Cu^{2+}. To test the system response to the standard mass-to-charge evaluation procedure, we have performed EQCN measurements using a Au|BSA electrode in 5 mM $CuSO_4$+5 mM H_2SO_4+ 9.6×10^{-8} M BSA, with potential waveform including scan from $E_1=0.6$ V to $E_2=0.15$ V at $v=50$ mV/s, holding at $E_2=0.15$ V for $\tau_{dep}=5$ s, and a scan to $E_3=0.6$ V at $v=50$ mV/s. The EQCN characteristics of *i–E* and *m–E* are presented in Fig. 11A, curves 1 and 2, respectively. It is seen that the mass cycle is reversible and the loss of mass due to diffusion of reactants to the bulk solution is negligible. The initial small mass decrease in the potential range from $E=0.6$ V to $E=0.32$ V can be attributed to the ligand expulsion [73–75] and double-layer effects [26], leading to the egress of anions (SO_4^{2-} and HSO_4^-) from the surface and double-layer region. The analysis of mass vs. integrated charge *m–Q* is presented in Fig. 11B, curve 1. The theoretical slope can be calculated from the formula [26]: $(\partial m/\partial Q)=-M/(nF)$, where *M* is the reaction molmass (the molar mass gain or loss of electrodic film due to the reactants attachment or detachment from the film) and *n* is the number of electrons exchanged in the reaction. Thus, for a 2-electron Cu(II) discharge and electrodissolution of Cu^0: $S_{Cu,2}=(\partial m/\partial Q)=-0.329$ ng/μC. In Fig. 11B, curve 1, the sections A and C show a slope $(\partial m/\partial Q)$ which is smaller than the theoretical $S_{Cu,2}$. The smaller slope means that in the region of section A the copper ion reduction process partially involves Cu(II) ions trapped or bound in BSA film, which results in the mass deficiency with respect to the charge used in the process. The second region of mass deficiency is the region of section C, where during the oxidation process, part of the Cu(II) ions formed is not leaving the BSA film either because of interactions with BSA, requirements of Donnan membrane equilibria, or slowness of the mass transport. If we reject regions A and C from further considerations and calculate the effective number of electrons involved: $n=M/[F(\partial m/\partial Q)]$ only for regions B and D, we find that the slopes $(\partial m/\partial Q)$ are: −0.408 and −0.391 ng/μC, respectively, which correspond to $n=1.61$ and $n=1.68$ for sections B and D. We can assume the average value of *n* for these two sections to be: $n=1.65$. It is, therefore, possible that Cu-u.p.d. retains a partial charge of $\xi=2-n=+0.35$. By substituting the new value of *n* for *z* in Eq. (6), one can correct the interaction coefficient $g_{M,X}$ determined from the slope $(\partial E_p/\partial\Theta_{BSA})$ to obtain: $g^*_{M,X}=-4.62$, which is now very close to the critical value of −4. The resemblance of Cu-u.p.d. desorption voltammograms observed in this work for Au|BSA to those obtained for ethanethiol SAM on Au [63] suggests that a similar strong interactions between Cu_{ad} and adsorbed ethanethiol may exist. This is justified by very strong interactions of thiols with copper and other metals [76–90]. From our measurements, it follows that BSA interactions with Cu_{ad} are almost as strong as those of ethanethiol (according to Eq. (6); the stronger the attractive interaction is, the more positive the shift of E_p becomes). Further studies are needed to elucidate in more detail the observed phenomena in these systems. In a similar wedging process of metal adatoms, which we have found previously in supported phospholipid membranes with embedded gramicidin ion channels [69], a full monolayer of Tl-u.p.d. was formed underneath a lipid film. In this case, the wedging of Tl_{ad} was found to induce a temporary lipid film lifting. Unlike this, the Cu adatoms here have not induced any BSA film dynamic transformations, which could be revealed in the *m–E* or *m–t* characteristics, such as those observed in Cd-adatoms/NO_3^- systems [9].

4. Conclusions

The investigations of adsorption of a model protein, BSA, on Au electrodes were performed using the Cu adatom probe method and Electrochemical Quartz Crystal Nanobalance (EQCN) technique in an attempt to explore the interfacial phenomena in a system where large biological molecules interact with small metal adatoms. We have found that the formation of a dense protein adsorption film can block completely only a bulk Cu^0 deposition process. In contrast to that, the mass associated with Cu-u.p.d. decreases during the adsorption of BSA only to ca. 50% of that in the absence of BSA, indicating that Cu adatoms can wedge into the space between the surface Au atoms and the adsorbed BSA molecules. We have found that the degree of

penetration of Cu adatoms can be controlled by the applied deposition potential. By selecting a sufficiently cathodic potential, we were able to deposit a full Cu-u.p.d. monolayer, independent of the BSA surface coverage extending from $\Theta_{BSA}=0$ to $\Theta_{BSA}\approx 1$. Our interpretation of the positive shift of Cu_{ad} desorption peak potential E_p, observed in the presence of adsorbed BSA, is based on the Frumkin exchange interaction forces between Cu_{ad} and BSA_{ad}, defined according to our earlier theoretical model [61], expanded here to include adsorbed species in two monolayers. This expansion is possible owing to the fast rate of Cu adatom penetration in the interfacial region. From the analysis of E_p vs. Θ_{BSA} plots, the presence of strong attractive interactions between Cu_{ad} and BSA_{ad} was found. The wedging effects demonstrated in this work are similar in nature to those observed for Cu-u.p.d. on the ethanethiol SAM on Au (111) by Espandiu et al. [63] and metal adatoms on a tripeptide glutathione adsorbed on gold [48,49]. No dynamic transformations of BSA film, such as those observed for the Cd-adatoms/NO_3^- system [9], were induced by Cu adatoms.

Acknowledgements

This work was supported by the National Science Foundation Grant No. CCLI-0126402, the Cottrell College Science Award No. CC-4733 and by the FUSR Grant, SUNY at Potsdam.

References

[1] E.F. Bowden, F.M. Hawkridge, H.N. Blount, J. Electroanal. Chem. 161 (1984) 355.
[2] F.A. Armstrong, K.J. Brown, J. Electroanal. Chem. 219 (1987) 319.
[3] F.A. Armstrong, Elektrokhimiya 38 (2002) 58.
[4] I. Willner, N. Lapidot, A. Riklin, R. Kasher, E. Zahavy, Eugenii Katz, J. Am. Chem. Soc. 116 (1994) 1428.
[5] J. Halamek, M. Hepel, P. Skladal, Biosens. Bioelectron. 16 (2001) 253.
[6] J. Pribyl, M. Hepel, J. Halamek, P. Skladal, Sens. Actuators, B 91 (2003) 333.
[7] P. Skladal, J. Braz. Chem. Soc. 14 (2003) 491.
[8] M. Hepel, Electroanalysis 17 (2005) 1401.
[9] M. Stobiecka, M. Hepel, J. Radecki, Electrochim. Acta 50 (2005) 4873.
[10] C. Tanford, J. Am. Chem. Soc. 74 (1952) 6039.
[11] I. Kolthoff, A. Anastasi, B. Tan, J. Am. Chem. Soc. 80 (1958) 3235.
[12] R. Cecil, P.D.J. Weitzman, Biochem. J. 93 (1964) 1.
[13] G. Markus, J. Biol. Chem. 239 (1964) 4163.
[14] S. Leach, A. Meschers, D. Swanepoel, Biochemistry 4 (1965) 23.
[15] V. Zahn, H. Gattner, Z. Physiol. Chem. 349 (1968) 373.
[16] L. Holleck, J.M. Abd el Kader, A.M. Shams el Din, J. Electroanal. Chem. 17 (1968) 401.
[17] M. Bialowolska, B. Behr, J. Chodkowski, Rocz. Chem. 42 9 (1968) 935.
[18] B. Behr, M. Bialowolska, J. Chodkowski, J. Electroanal. Chem. 46 (1973) 223.
[19] B. Kuznetsov, G. Shumakovich, Bioelectrochem. Bioenerg. 1 (1973) 345.
[20] M.T. Stankovich, A.J. Bard, J. Electroanal. Chem. 85 (1977) 173.
[21] K.S.V. Santhanam, N. Jespersen, A.J. Bard, J. Am. Chem. Soc. 99 (1977) 274.
[22] M.T. Stankovich, A.J. Bard, J. Electroanal. Chem. 95 (1978) 189.
[23] J. Wang, G. Rivas, M. Jiang, X. Zhang, Langmuir 15 (1999) 6541.
[24] J. Wang, Electroanalytical Techniques in Clinical Chemistry and Laboratory Medicine (1988).
[25] J. Wang, Stripping Voltammetry, VCH Publishers, Deerfield Beach, Fl, 1985.
[26] M. Hepel, in: A. Wieckowski (Ed.), Interfacial Electrochemistry, M. Dekker, New York, 1999, pp. 599–631.
[27] Y. Cai, Q. Xie, A. Zhou, Y. Zhang, S. Yao, J. Biochem. Biophys. Methods 47 (2001) 209–219.
[28] C.M. Wu, L.Y. Lin, Sens. Actuators, B 110 (2005) 231.
[29] T. Haruyama, T. Sakai, K. Matsuno, Biomaterials 26 (2005) 4944–4947.
[30] P. Tengvall, A. Askendal, I. Lundstrom, Biomaterials 19 (1998) 935.
[31] M. Hepel, Z. Fijalek, in: R. Ottenbrite (Ed.), Polymeric Drugs and Drug Administration, ACS Symposium Series, Washington, DC, vol. 545, 1994, pp. 79–97.
[32] N.R. Cabilio, S. Omanovic, S.G. Roscoe, Langmuir 16 (2000) 8480.
[33] S. Omanovic, S.G. Roscoe, J. Colloid Interface Sci. 227 (2000) 452.
[34] S. Omanovic, S.G. Roscoe, Langmuir 15 (1999) 8315.
[35] T. Arnebrant, T. Nylander, J. Colloid Interface Sci. 111 (1986) 529.
[36] B.A. Ivarsson, P. Hegg, K.I. Lundstrom, U. Jonsson, Colloids Surf. 13 (1985) 169.
[37] T. Arnebrant, B. Ivarsson, K. Larsson, I. Lundstrom, T. Nylander, Prog. Colloid & Polym. Sci. 70 (1985) 62.
[38] P. Tengvall, A. Askendal, I. Lundstrom, J. Biomed. Mater. Res. 57 (2001) 285.
[39] R.G. Lee, S.W. Kim, J. Biomed. Mater. Res. 8 (1974) 251.
[40] R.C. Eberhart, L.D. Prokop, J. Wissenger, M.A. Wilkov, Trans. Am. Soc. Artif. Intern. Organs 23 (1977) 134.
[41] A.M. Moulin, S.J. O'Shea, R.A. Badley, P. Doyle, M.E. Wellend, Langmuir 15 (1999) 8776.
[42] J.C. O'Brien, J.T. Stickney, M.D. Porter, Langmuir 16 (2000) 9559.
[43] Z.Q. Feng, S. Imabayashi, T. Kakiuchi, K. Niki, J. Chem. Soc. Faraday Trans. 93 (1997) 1367.
[44] S. Lecompte, H. Wackerbarth, T. Soulimane, J. Am. Chem. Soc. 120 (1998) 7381.
[45] S. Bruckenstein, M. Shay, J. Electroanal. Chem. 188 (1985) 131.
[46] A.M.O. Brett, A.M. Chiorcea, Electrochem. Commun. 5 (2003) 178.
[47] A.V. Elgersma, R.L.J. Zsom, J. Lyklema, W. Norde, J. Colloid Interface Sci. 152 (1992) 410.
[48] M. Hepel, E. Tewksbury, J. Electroanal. Chem. 552 (2003) 291.
[49] M. Hepel, E. Tewksbury, Electrochim. Acta 49 (2004) 3827.
[50] M. Hepel, Electrochim. Acta 41 (1996) 63.
[51] M. Hepel, W. Janusz, Electrochim. Acta 45 (2000) 3785.
[52] M. Hepel, F. Mahdavi, Microchem. J. 56 (1997) 54.
[53] M. Hepel, L. Dentrone, Electroanalysis 7 (1996) 1.
[54] M. Hepel, L. Dentrone, E. Seymour, in: I. Node, D.N. Rubingh (Eds.), Polymer Solutions, Blends, and Interfaces, Elsevier Science Publishers, 1992, pp. 385–405.
[55] J. Hepel, S. Bruckenstein, M. Hepel, Microchem. J. 55 (1997) 179.
[56] M. Hepel, J. Electrochem. Soc. 145 (1998) 124.
[57] J. Luo, H. Huang, Z. Lin, M. Hepel, in: J. Rubinson, H. Mark (Eds.), Conducting Polymers and Polymer Electrolytes. From Biology to Photovoltaics, ACS Symp. Series, vol. 832, Oxford University Press, 2002, p. 113.
[58] M. Hepel, E. Seymour, D. Yogev, J.H. Fendler, Chem. Mater. 4 (1992) 209.
[59] J.E.I. Wright, N.P. Cosman, K. Fatih, S. Omanovic, S.G. Roscoe, J. Electroanal. Chem. 564 (2004) 185.
[60] Y. Cai, Q. Xie, A. Zhou, Y. Zhang, S. Yao, J. Biochem. Biophys. Methods 47 (2001) 209–219.
[61] M. Hepel, Electroanalysis 2 (1990) 319.
[62] M. Hepel, I. Kumarihamy, J. Electroanal. Chem., (submitted for publication).
[63] M.J. Espandiu, M.A. Schneeweis, D.M. Kolb, Langmuir 15 (1999) 7802.
[64] G. Sauerbrey, Z. Phys. 155 (1959) 206.
[65] S. Trasatti, O.A. Petrii, Pure Appl. Chem. 63 (1991) 711.
[66] M. Hepel, E. Cateforis, Electrochim. Acta 46 (2001) 3801.
[67] M. Hepel, S. Bruckenstein, Electroanalysis 1 (1989) 311.
[68] P.J. Sadler, A. Tucker, J.H. Viles, Eur. J. Biochem. 220 (1994) 193.
[69] M. Hepel, J. Electroanal. Chem. 509 (2001) 90.
[70] D.R. Jung, A.W. Czanderna, Crit. Rev. Solid State Mater. Sci. 19 (1994) 1.
[71] G.C. Herdt, D.R. Jung, A.W. Czanderna, Prog. Surf. Sci. 50 (1995) 103.
[72] E.D. Eliadis, R.G. Nuzzo, A.A. Gewirth, R.C. Alkire, J. Electrochem. Soc. 144 (1997) 96.
[73] M. Hepel, S. Bruckenstein, Electrochim. Acta 34 (1989) 1499.

[74] M. Hepel, K. Kanige, S. Bruckenstein, J. Electroanal. Chem. 266 (1989) 409.
[75] M. Hepel, K. Kanige, S. Bruckenstein, Langmuir 6 (1990) 1063.
[76] R.G. Nuzzo, D.L. Alara, J. Am. Chem. Soc. 105 (1983) 4481.
[77] M.D. Porter, T.B. Bright, D.L. Alara, C.D.E. Chidsey, J. Am. Chem. Soc. 109 (1987) 3559.
[78] L. Strong, G.M. Whitesides, Langmuir 4 (1988) 546.
[79] C.B. Bain, G.M. Whitesides, Science 240 (1988) 62.
[80] C.D. Bain, E.B. Troughton, Y.T. Tao, J. Evall, G.M. Whitesides, R.G. Nuzzo, J. Am. Chem. Soc. 111 (1989) 321.
[81] G.M. Whitesides, P.E. Laibinis, Langmuir 6 (1990) 87.
[82] C.A. Widrig, C. Chung, M.D. Porter, J. Electroanal. Chem. 310 (1991) 335.
[83] C. Miller, P. Cuendet, M. Gratzel, J. Phys. Chem. 95 (1991) 877.
[84] C. Miller, M. Gratzel, J. Phys. Chem. 95 (1991) 5225.
[85] P.E. Laibinis, G.M. Whitesides, D.L. Alara, Y.T. Tao, A.N. Parkin, R.G. Nuzzo, J. Am. Chem. 113 (1991) 7152.
[86] P. Krysinski, R.V. Chamberlain, M. Majda, Langmuir 10 (1994) 4286.
[87] W. Pan, C.J. Durning, N.J. Turro, Langmuir 12 (1996) 4469.
[88] T. Komura, T. Yamaguchi, K. Takahashi, H. Terasawa, J. Electroanal. Chem. 481 (2000) 183.
[89] K. Sugihara, K. Shimazu, K. Uosaki, Langmuir 16 (2000) 7101.
[90] M. Hepel, M. Scendo, in: J. Stickney, M. Soriaga (Eds.), Thin Films: Preparation, Characterization, and Applications, Kluwer Academic/Plenum Publishers, New York, 2001.